Stereochemically non-rigid transition metal complexes of 2,6-bis[(1-phenylimino)ethyl]pyridine (BIP)
Part 2. Dynamic NMR studies of fac-[ReX(CO)₃(BIP)] (X = Cl, Br, or I). Crystal structure of fac-[ReBr(CO)₃(BIP)]

Keith G. Orrell [a,*], Anthony G. Osborne [a], Vladimir Šik [a], Mateus Webba da Silva [a],
Michael B. Hursthouse [b], David E. Hibbs [b], K.M. Abdul Malik [b], Nikolay G. Vassilev [c]

[a] *Department of Chemistry, University of Exeter, Exeter EX4 4QD, UK*
[b] *School of Chemistry and Applied Chemistry, University of Wales, Cardiff CF1 3TB, UK*
[c] *Institute of Organic Chemistry, Bulgarian Academy of Sciences, Sofia 1113, Bulgaria*

Abstract

The complexes fac-[ReX(CO)₃(BIP)] (X = Cl, Br or I; BIP = 2,6-bis[(1-phenylimino)ethyl]pyridine) have been synthesised and characterised as involving BIP as a bidentate chelate ligand. In solution the ligand exists in three conformational forms, namely E,E- and both *distal* and *proximal* E,Z-isomers. 2D-EXSY NMR has been used to measure 1,4-metallotropic shifts of the ReX(CO)₃ moiety between equivalent E,E forms, E,Z-isomerisation of the pendant imine function and restricted C–C rotation of the pendant arm of the BIP ligand. Activation energies $\Delta G^{\neq}$ (298.15 K) for all these processes are of comparable magnitude, in the range 79–88 kJ mol^{-1}, and are essentially halogen independent. Restricted rotation of the phenyl ring attached to the Re-coordinated nitrogen was also detected with $\Delta G^{\neq} = 67.3 \pm 0.2$ kJ mol^{-1}. A crystal structure of fac-[ReBr(CO)₃(BIP)] confirms the E-conformation of the pendant imine function with its N atom *cis* to the pyridyl nitrogen.

Keywords: Rhenium; Bis-imine ligand; Fluxionality; 2D-EXSY NMR

1. Introduction

The ligands 2,2':6',2"-terpyridine (terpy) [1,2], 2,6-bis(pyrazol-1-yl)pyridine (bppy) [3], 2,6-bis[(3,5-dimethyl)pyrazol-1-yl]pyridine (tmbppy) [3] and 2-(3,5-dimethylpyrazol-1-yl)-6-(pyrazol-1-yl)pyridine (dmbppy) [3] react with [ReX(CO)₅] to form stable octahedral complexes of type fac-[ReX(CO)₃(L–L)] (X = Cl, Br, I; L–L is a bidentate chelate ligand), in which the potentially terdentate ligands are acting in a biden-

tate chelate fashion. In solution these complexes are fluxional with the ligand oscillating between bidentate bonding modes by a twist mechanism involving the breaking/making of two Re–N bonds. In Part 1 [4] we described the synthesis and solution fluxionality of the square planar complexes [M(C₆F₅)₂(BIP)] (M = Pd^{II} or Pt^{II}, BIP = 2,6-bis[(1-phenylimino)ethyl]pyridine). Here we describe the results of our investigations into the synthesis, structures and dynamic behaviour in solution of the complexes fac-[ReX(CO)₃(BIP)] (X = Cl, Br, and I). The bromide of this series has been characterised previously but the occurrence of stereoisomers and the dynamic behaviour in solution was not reported [5,6].

* Corresponding author.

2. Results

The complexes *fac*-[ReX(CO)$_3$(BIP)] (X = Cl, Br and I) were all prepared in a similar manner from the reaction of BIP with the appropriate pentacarbonyl halide in benzene. The reactions were monitored by infrared spectroscopy in the carbonyl stretching region (2200–1600 cm^{-1}). The complexes were isolated in very high yields as air-stable, orange–red solids that melted at temperatures in the range 225–259 °C (Table 1).

Mass spectra of these complexes were measured (Table 1). For the chloride and bromide the fragmentation pattern shows the corresponding molecular ion [M]$^+$ whereas for the iodide the highest m/z value represents an ion corresponding to the loss of one carbonyl group [M–CO]$^+$. For all cases the observed and calculated isotope patterns are in agreement.

In the carbonyl stretching region of the infrared spectra the complexes show three almost equally intense peaks consistent with a *facial* arrangement of the carbonyl groups. This indicates that the ligand BIP substitutes two equatorial carbonyl groups of the [ReX(CO)$_5$] reactant. Confirmation that BIP is acting as a bidentate chelate ligand arises from the ^{1}H NMR and crystal structure studies (see below).

2.1. X-ray crystallography

The crystal structure of [ReBr(CO)$_3$(BIP)] was determined. Atomic fractional coordinates are given in Table 2. A view of the molecule indicating the numbering scheme adopted is shown in Fig. 1. The structure confirms the octahedral coordination for the Re atom, the *facial* disposition of the carbonyl groups and that the pendant imine function is in the E conformation with its

nitrogen atom *cis* to the pyridyl nitrogen. Bond distances and bond angles are listed in Table 3.

The main distortion to the octahedral geometry at Re arises from the small 'bite-angle' of BIP, N(1)–Re–N(3) 74.0°. The Re–N distances are unequal with Re–N(1) 2.226 and Re–N(3) 2.160 Å. This is in contrast to the situation found in complexes in which BIP is acting as a terdentate ligand, where the shortest metal–nitrogen distance is to the pyridyl nitrogen [6–8]. This changeover in relative metal–nitrogen bond lengths between bidentate and terdentate forms of a ligand is also found in metal complexes of 2,2':6',2"-terpyridine (terpy) [9]. The expected lengthening of an imine bond upon coordination to a metal is shown by comparing N(3)–C(13) 1.300 Å with N(2)–C(6) 1.254 Å.

2.2. ^{1}H and ^{13}C NMR studies

^{1}H NMR spectra for these complexes were taken at −10 °C in CDCl$_3$. Chemical shifts (δ) and coordination shifts ($\Delta\delta$) are recorded in Table 4. Coordination shifts of most aromatic hydrogens are positive, particularly those for the *ortho* phenyl protons and the 4-position pyridyl protons, but significant low frequency coordination shifts occur for the *meta* signals of the pyridyl unit (H$_G$ and H$_I$). These low frequency shifts are the result of the preferred conformation of the terminal imine C=N bonds, relative to the pyridyl ring, changing from a *trans* to a *cis* orientation on metal coordination. All *ortho* protons of the phenyl rings show significant high frequency coordination shifts, particularly signal H$_A$. The *para* protons (H$_C$ and H$_M$) can be used to distinguish between the two types of phenyl groups. The proton of the ring attached to the metal-bound nitrogen (H$_C$) shows the effect of coordination to rhenium(I) by a high frequency coordination shift of

Table 1
Analytical data for the complexes *fac*-[ReX(CO)$_3$(BIP)] (X = Cl, Br, or I)

Complex	M.p. (°C)	Yield [a] (%)	ν(CO) [b]	Analysis [c] (%)			m/z [d]			
				C	H	N	[M]$^+$	[M − CO]$^+$	[M − (CO)$_2$]$^+$	[M − (CO)$_3$]$^+$
[ReCl(CO)$_3$(BIP)]	225/7	86.7	2029vs 1933s 1905s	46.56 (45.96)	3.09 (3.07)	6.79 (6.49)	620	591 [e]	563	535
[ReBr(CO)$_3$(BIP)]	253/5	91.5	2029vs 1933s 1905s	43.45 (43.24)	2.86 (2.76)	6.34 (6.10)	664	635 [e]	607	579
[ReI(CO)$_3$(BIP)]	256/9 (dec.)	95.7	2028vs 1935s 1908s	40.57 (40.62)	2.70 (2.63)	5.91 (5.39)	—	683	655	625 [e]

[a] Yield quoted relative to metal-containing reactant.
[b] Recorded in CHCl$_3$ solution; s = strong, v = very.
[c] Calculated values in parentheses.
[d] LSIMS technique.
[e] Most abundant.

Table 2

Atomic coordinates ($\times 10^4$) and equivalent isotropic displacement parameters ($\mathring{A}^2 \times 10^3$) for $C_{24}H_{19}BrN_3O_3Re$

Atom	x	y	z	U_{eq}
Re(1)	2006.0(3)	614.6(3)	1565.2(2)	15(1)
Br(1)	676.3(10)	1674.8(7)	2949.9(6)	20(1)
N(2)	3838(8)	−2743(6)	3417(5)	21(2)
N(1)	4122(7)	−47(6)	2782(5)	15(1)
N(3)	3530(8)	1989(6)	985(5)	15(1)
C(10)	1584(12)	−5695(9)	3837(10)	43(3)
C(9)	2143(11)	−5578(8)	4787(8)	36(2)
C(8)	2841(11)	−4603(8)	4674(7)	30(2)
C(7)	3024(9)	−3724(7)	3594(7)	20(2)
C(12)	2505(11)	−3862(9)	2637(8)	32(2)
C(11)	1769(12)	−4818(10)	2763(9)	43(3)
C(5)	4445(10)	−1092(7)	3694(7)	21(2)
C(4)	5744(10)	−1359(8)	4447(7)	24(2)
C(3)	6790(11)	−539(8)	4242(7)	29(2)
C(2)	6484(9)	510(8)	3305(7)	24(2)
C(1)	5173(9)	756(7)	2596(7)	19(2)
C(6)	3378(9)	−2029(7)	3910(6)	18(2)
C(13)	4812(10)	1870(7)	1589(7)	19(2)
C(20)	5918(10)	2793(8)	1280(8)	31(2)
C(14)	3089(9)	3023(7)	−30(6)	17(2)
C(15)	2258(10)	4097(7)	65(7)	20(2)
C(16)	1799(11)	5084(9)	−907(8)	33(2)
C(17)	2175(11)	5054(8)	−1982(8)	33(2)
C(18)	3001(13)	4016(9)	−2056(8)	37(2)
C(19)	3454(11)	2996(8)	−1095(7)	28(2)
C(23)	330(10)	1520(8)	450(7)	23(2)
C(24)	614(10)	−599(8)	2174(7)	22(2)
O(3)	3438(7)	−561(6)	−88(5)	31(2)
O(1)	−262(7)	−1289(6)	2479(6)	35(2)
O(2)	−679(8)	2099(6)	−224(6)	38(2)
C(22)	2928(10)	−133(7)	543(7)	23(2)
C(21)	1928(11)	−1989(8)	4717(8)	32(2)

U_{eq} is defined as one third of the trace of the orthogonalized U_{ij} tensor.

0.18 ppm in all three complexes, whereas the proton of the pendant phenyl group shows virtually no coordination shift. High frequency coordination shifts for the *meta* protons, H_B and H_D, and low frequency coordina-tion shifts for H_L and H_N are all of much smaller magnitude.

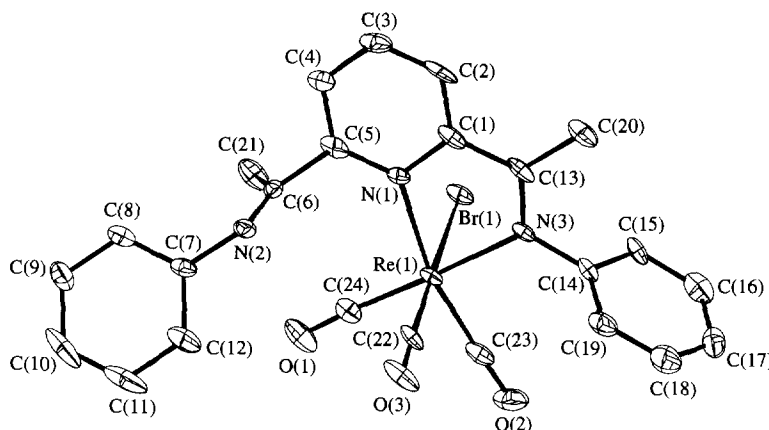The assignments in Table 4 were based on $^1H–^1H$ correlated spectroscopy (COSY) and nuclear Over-

Fig. 1. A view of the crystal structure of *fac*-[ReBr(CO)$_3$(BIP)] showing the atom labelling.

Table 3
Bond lengths (Å) and angles (°) for $C_{24}H_{19}BrN_3O_3Re$

Re(1)–C(22)	1.904(9)	Re(1)–C(23)	1.904(9)
Re(1)–C(24)	1.937(8)	Re(1)–N(3)	2.160(6)
Re(1)–N(1)	2.226(6)	Re(1)–Br(1)	2.6373(11)
N(2)–C(6)	1.254(10)	N(2)–C(7)	1.423(10)
N(1)–C(5)	1.350(10)	N(1)–C(1)	1.373(10)
N(3)–C(13)	1.300(10)	N(3)–C(14)	1.425(10)
C(10)–C(9)	1.384(14)	C(10)–C(11)	1.39(2)
C(9)–C(8)	1.378(12)	C(8)–C(7)	1.396(12)
CC(7)–C(12)	1.391(12)	C(12)–C(11)	1.371(13)
C(5)–C(4)	1.389(11)	C(5)–C(6)	1.508(11)
C(4)–C(3)	1.384(12)	C(3)–C(2)	1.367(12)
C(2)–C(1)	1.367(11)	C(1)–C(13)	1.463(12)
C(6)–C(21)	1.524(10)	C(13)–C(20)	1.504(11)
C(14)–C(19)	1.373(11)	C(14)–C(15)	1.417(11)
C(15)–C(16)	1.367(13)	C(16)–C(17)	1.388(13)
C(17)–C(18)	1.365(13)	C(18)–C(19)	1.378(13)
C(23)–O(2)	1.156(10)	C(24)–O(1)	1.150(10)
O(3)–C(22)	1.136(10)		
C(22)–Re(1)–C(23)	87.8(3)	C(22)–Re(1)–C(24)	88.4(3)
C(23)–Re(1)–C(24)	87.4(3)	C(22)–Re(1)–N(3)	95.0(3)
C(23)–Re(1)–N(3)	93.9(3)	C(24)–Re(1)–N(3)	176.4(3)
C(22)–Re(1)–N(1)	97.4(3)	C(23)–Re(1)–N(1)	167.2(3)
C(24)–Re(1)–N(1)	104.4(3)	N(3)–Re(1)–N(1)	74.0(2)
C(22)–Re(1)–Br(1)	178.8(3)	C(23)–Re(1)–Br(1)	91.0(2)
C(24)–Re(1)–Br(1)	91.5(2)	N(3)–Re(1)–Br(1)	85.1(2)
N(1)–Re(1)–Br(1)	83.8(2)	C(6)–N(2)–C(7)	121.8(7)
C(5)–N(1)–C(1)	117.0(7)	C(5)–N(1)–Re(1)	128.6(5)
C(1)–N(1)–Re(1)	114.3(5)	C(13)–N(3)–C(14)	121.2(6)
C(13)–N(3)–Re(1)	119.1(5)	C(14)–N(3)–Re(1)	119.6(5)
C(9)–C(10)–C(11)	118.5(8)	C(8)–C(9)–C(10)	120.8(9)
C(9)–C(8)–C(7)	120.4(8)	C(12)–C(7)–C(8)	118.6(8)
C(12)–C(7)–N(2)	118.3(7)	C(8)–C(7)–N(2)	122.9(7)
C(11)–C(12)–C(7)	120.4(9)	C(12)–C(11)–C(10)	121.2(9)
N(1)–C(5)–C(4)	123.0(7)	N(1)–C(5)–C(6)	119.3(7)
C(4)–C(5)–C(6)	117.7(7)	C(3)–C(4)–C(5)	119.0(8)
C(2)–C(3)–C(4)	118.0(8)	C(1)–C(2)–C(3)	121.4(8)
C(2)–C(1)–N(1)	121.5(8)	C(2)–C(1)–C(13)	122.7(7)
N(1)–C(1)–C(13)	115.8(7)	N(2)–C(6)–C(5)	115.0(7)
N(2)–C(6)–C(21)	129.6(7)	C(5)–C(6)–C(21)	115.4(6)
N(3)–C(13)–C(1)	116.4(7)	N(3)–C(13)–C(20)	123.2(8)
C(1)–C(13)–C(20)	120.3(7)	C(19)–C(14)–C(15)	119.6(8)
C(19)–C(14)–N(3)	121.3(7)	C(15)–C(14)–N(3)	119.1(7)
C(16)–C(15)–C(14)	119.3(8)	C(15)–C(16)–C(17)	120.9(9)
C(18)–C(17)–C(16)	118.9(9)	C(17)–C(18)–C(19)	121.8(9)
C(14)–C(19)–C(18)	119.4(9)	O(2)–C(23)–Re(1)	178.1(7)
O(1)–C(24)–Re(1)	176.2(8)	O(3)–C(22)–Re(1)	178.0(8)

hauser effect (NOE) difference studies. For example, irradiation of the signal Me_J gave two strong positive NOEs due to the signals H_I and H_K/H_O. This indicates that the nitrogen in the pendant part of the ligand is in a cis orientation relative to the pyridyl nitrogen and, furthermore, that the phenyl ring is undergoing rapid rotation around the $N–C_{ipso}$ bond. Irradiation of signal Me_F gave a strong positive NOE build up in signal H_G. This indicates a cis conformation between the metal-bound nitrogen and the pyridyl nitrogen. However, no NOE was observed for the ortho signals H_A/H_E of the

phenyl group. This may be due to the arrested rotation of this phenyl group, which has a preferred orientation almost perpendicular to the chelate plane. The anisochronous nature of H_A and H_E supports this proposal.

In the solution spectra of these complexes there is evidence of two other species, which could not be separated chromatographically. Since the elemental analyses for the complexes were reliable (Table 1) and both these minor species were involved in exchange processes with the major species, both were assumed to

Table 4
^{1}H NMR data ^{a} for the aromatic region for complexes fac-[ReX(CO)$_3$(BIP)] (Cl, Br or I) in CDCl$_3$ at $-10\,^\circ$C

Com-pound		δ_A J_{AB} J_{AC}	δ_B J_{BC} J_{BD}	δ_C J_{CD} J_{CE}	δ_D J_{DC} J_{DB}	δ_E J_{ED} J_{EC}	δ_G J_{GH} J_{GI}	δ_H J_{HG} —	δ_I J_{IH} J_{IG}	δ_K J_{KL} J_{KM}	δ_L J_{LM} J_{LN}	δ_M J_{MN} J_{MO}	δ_N J_{NM} J_{NL}	δ_O J_{ON} J_{OM}
BIP		dm 6.88	tm 7.40	tt 7.14	tm 7.40	dm 6.88	d 8.37	t 7.88	d 8.37	dm 6.88	tm 7.40	tt 7.14	tm 7.40	dm 6.88
		8.2	8.2	8.2	8.2	8.2	7.8	7.8	7.8	8.2	8.2	8.2	8.2	8.2
		—	—	1.1	—	—	—	—	—	—	—	1.1	—	—
Cl		dm 7.29	m 7.49	tt 7.32	m 7.49	dm 7.02	dd 8.03	t 8.18	dd 7.84	dm 7.03	t 7.38	tt 7.17	t 7.38	dm 7.03
		8.3	—	6.9	—	8.3	7.8	7.8	7.89	8.5	8.5	6.9	8.5	8.5
		—	—	1.1	—	—	1.1	—	1.1	—	—	1.1	—	—
	Δδ	0.41	0.09	0.18	0.09	0.14	−0.34	0.30	−0.53	0.15	−0.02	0.03	−0.02	0.15
Br		dm 7.35	m 7.49	tt 7.32	m 7.49	dm 7.03	dd 8.04	t 8.17	dd 7.73	dm 7.04	t 7.38	tt 7.15	t 7.38	dm 7.04
		8.3	—	7.9	—	8.3	7.8	7.8	7.8	8.5	8.5	6.9	8.5	8.5
		—	—	1.1	—	—	1.3	—	1.3	—	—	1.1	—	—
	Δδ	0.47	0.09	0.18	0.09	0.15	−0.33	0.29	−0.64	0.16	−0.02	0.01	−0.02	0.16
I		dm 7.32	m 7.48	tt 7.32	m 7.49	dm 7.03	dd 8.05	t 8.16	dd 7.70	dm 7.05	t 7.38	tt 7.15	t 7.38	dm 7.05
		8.4	—	7.4	—	8.4	7.8	7.8	7.8	8.4	8.4	6.9	8.4	8.4
		—	—	1.1	—	—	1.3	—	1.3	1.2	—	1.0	—	1.2
	Δδ	0.44	0.08	0.18	0.09	0.15	−0.32	0.28	−0.67	0.17	−0.02	0.01	−0.02	0.17

^{a} Chemical shifts δ relative to TMS, $\delta = 0$; coordination shifts $\Delta\delta = \delta_{complex} - \delta_{ligand}$; s = singlet, d = doublet, t = triplet, m = multiplet. Scalar couplings in hertz.

be isomers of the major product (Fig. 2). The major species is thought to be an E,E-isomer as exists in the solid state (Fig. 1). The minor species are thought to arise from different orientations of the Z-isomer of the pendant arm of the BIP ligand. An E,Z-isomer induces strong steric effects due to the pendant phenyl group.

The halide and the pendant N-phenyl group may be either on the same side of the chelate plane, the *proximal E,Z*-isomer, or on opposite sides, the *distal E,Z*-isomer. These species would be chemically and magnetically inequivalent. The more abundant is expected to be the one in which there is less steric interaction with the
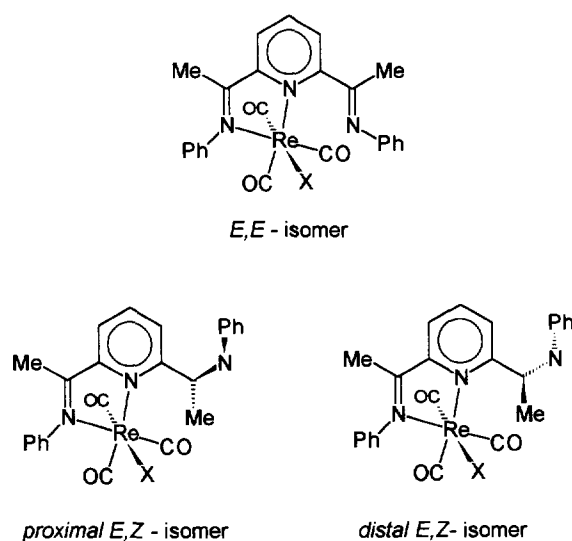
E,E - isomer

proximal E,Z - isomer   *distal E,Z*- isomer

Fig. 2. The proposed solution isomers of the complexes fac-[ReX(CO)$_3$(BIP)] (X = Cl, Br or I).

Table 5

^{1}H NMR data ^{a} of methyl region for complexes *fac*-[ReX(CO)$_3$(BIP)] (X = Cl, Br, I) in CDCl$_2$ · CDCl$_2$ at 30 °C

Compound	*E,E*-isomer		*distal E,Z*-isomer		*proximal E,Z*-isomer	
	F	J	F′	J′	F″	J″
		Abundance (%)		Abundance (%)		Abundance (%)
[ReCl(CO)$_3$(BIP)]	2.45	2.52	2.37	2.92	2.41	2.89
		84.4		8.4		7.2
[ReBr(CO)$_3$(BIP)]	2.46	2.56	2.38	2.96	2.42	2.89
		84.0		9.2		6.8
[ReI(CO)$_3$(BIP)]	2.48	2.57	2.40	2.97	2.43	2.81
		93.8		4.6		1.6

^{a} Chemical shifts δ relative to TMS, $\delta = 0$.

pendant phenyl ring, namely the *distal E,Z*-isomer. The less abundant species, considered to be the *proximal* isomer, shows a slight abundance decrease with increase in radius of the halide (Table 5).

The ^{13}C NMR spectrum of *fac*-[ReI(CO)$_3$(BIP)] was measured at -10 °C in (CDCl$_2$)$_2$ (Table 6). Only the aromatic region was examined. Correlations of the ^{13}C and ^{1}H signals were derived from the 2D ^{1}H–^{13}C HMQC spectrum shown in Fig. 3. It is noteworthy that the nuclei at the *ortho* positions C$_2$ and C$_6$ are anisochronous (as indeed are the attached hydrogens H$_A$ and H$_E$, Table 4), whereas the *meta* C$_3$ and C$_5$ nuclei are isochronous. It was not possible to assign the quaternary carbons of the ligand. Signals for these nuclei appear at $\delta = 156.44$, 162.59, 149.71, 147.62, 174.83, and 167.57.

2.3. Dynamic NMR studies

A solution ^{1}H NMR 1D variable temperature study was performed in the range -15 to 140 °C to establish the fluxional nature of the various isomers in each of the complexes. The spectra for *fac*-[ReI(CO)$_3$(BIP)] are

shown in Fig. 4. For all three complexes the spectra showed that the major and the minor species underwent exchange to produce, at higher temperatures, a spectrum representative of a single rapidly exchanging species. In order to analyse the exchange and to extract kinetic data, 2D-EXSY spectra were performed on the methyl region of the ^{1}H spectra. The mixing times τ_m used for each temperature are shown in Table 7.

The 2D-EXSY spectrum of the methyl region of *fac*-[ReBr(CO)$_3$(BIP)] obtained at 50 °C is shown in Fig. 5. Signals F and J are due to the major species, the *E,E*-isomer. Of the minor species the slightly more populous (*distal E,Z*) is represented by signals F′ and J′, and the less populous (*proximal E,Z*) by F″ and J″. Cross-peak signals identified the exchanges F ⇌ J, F′ ⇌ F (and J′ ⇌ J), F″ ⇌ F (and J″ ⇌ J), F′ ⇌ F″ (and J′ ⇌ J″). All the exchange processes, identified by their first-order rate constants k_{ij}, are summarised in the scheme in Fig. 6. There is no observed exchange F′ ⇌ J′ or F″ ⇌ J″. The exchange F ⇌ J represents a metallotropic shift. The exchanges F′ ⇌ F and F″ ⇌ F represent the imine *E,Z*-isomerisation of the pendant part of the ligand (Fig. 6; 1 ⇌ 3 and 2 ⇌ 3 respectively). Finally, the exchanges F′ ⇌ F″ (and J′ ⇌ J″) correspond

Table 6

^{13}C NMR data ^{a} for the aromatic and carbonyl carbons of *fac*-[ReI(CO)$_3$(BIP)] in (CDCl$_2$)$_2$ at -10 °C

^{13}C	2	3	4	5	6	10	11	12
δ^{13}	121.70	129.96	127.82	129.96	120.09	127.47	139.93	126.34
C	17	18	19	20	21	CO$_{equatorial}$	CO$_{equatorial}$	CO$_{axial}$
δ	120.54	129.13	125.29	129.13	120.54	196.16	194.72	186.81

^{a} Chemical shifts δ relative to TMS, $\delta = 0$.
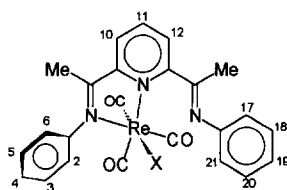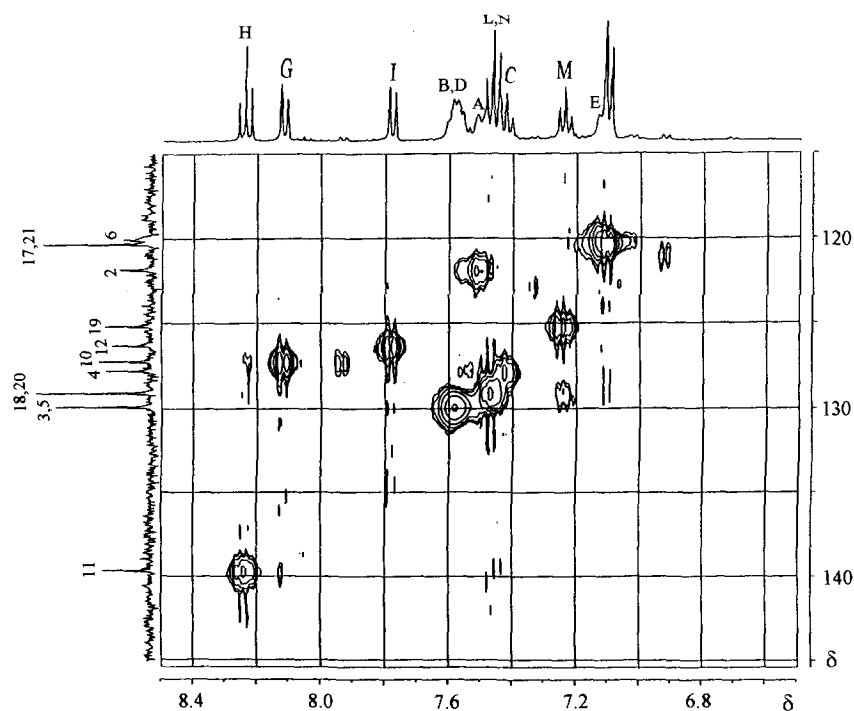
Fig. 3. The ^{1}H–^{13}C COSY HMQC spectrum of fac-[ReI(CO)$_3$(BIP)] in (CDCl$_2$)$_2$ at 30 °C.

to the restricted rotation of the C–C bond of the pendant part of the ligand; i.e. exchange between *distal E,Z*- and *proximal E,Z*-isomers (1 ⇌ 2, 5 ⇌ 6, Fig. 6). Exchange between both *proximal E,Z*-enantiomers (2 ⇌ 5) or *distal E,Z*-enantiomers (1 ⇌ 6) would involve both a metallotropic shift and *E,Z*-isomerisation and are unlikely exchange pathways.

2.3.1. Kinetic studies

The exchange processes were formulated as a six-site exchange problem. Each 2D-EXSY spectrum was con-

verted into a 6 × 6 intensity matrix I by integrating the area under each peak, the integrations being performed on the rows containing the most intense slices of the signals. Cross-peaks between the same diagonal signals must have the same intensity in a symmetrised 2D spectrum. Integral intensities of such pairs of cross-peaks measured on different rows were therefore adjusted to the same value. Furthermore, because of the equivalences of some of the exchange pathways, e.g. F′ ⇌ F″ and J′ ⇌ J″, etc., other 2D-EXSY signal intensities I were made equal, namely $I_{12} = I_{65}$, $I_{13} = I_{64}$, $I_{23} = I_{54}$,
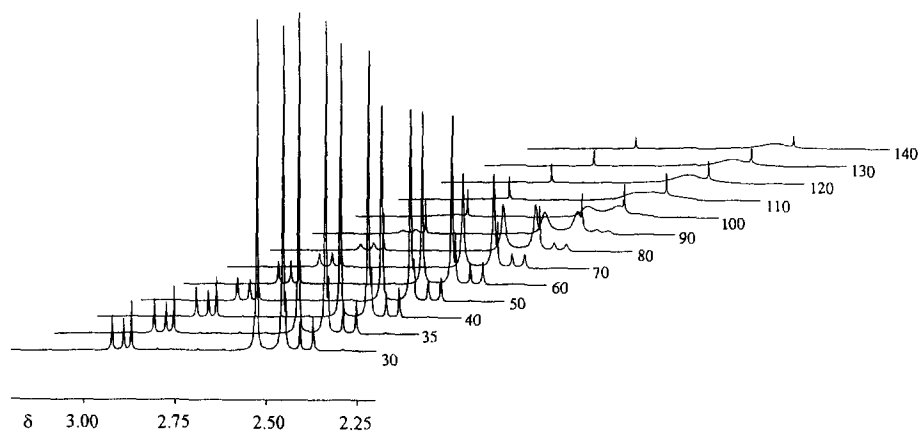

Fig. 4. 400 MHz ^{1}H NMR spectra (methyl region) of fac-[ReI(CO)$_3$(BIP)] in (CDCl$_2$)$_2$ in the temperature range 30–140 °C.
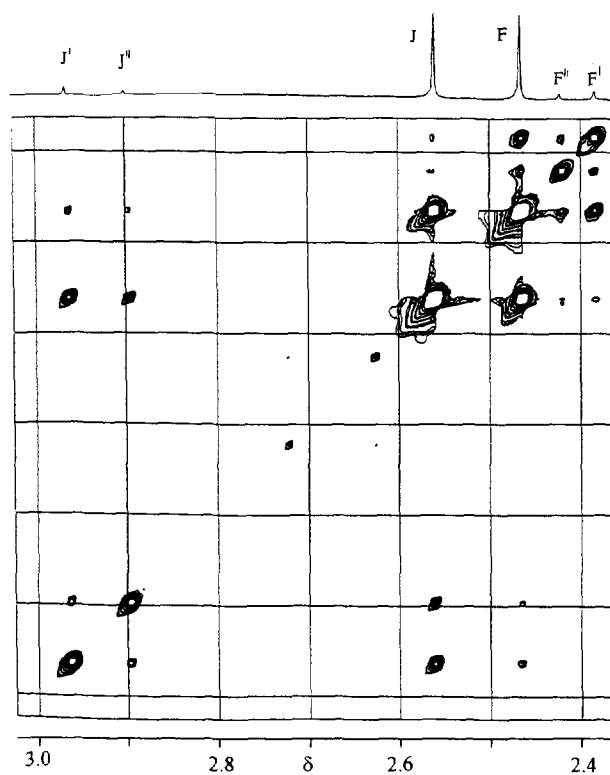
Fig. 5. 400 MHz ^{1}H NMR 2D-EXSY spectrum (methyl region) of fac-[ReBr(CO)$_3$(BIP)] in (CDCl$_2$)$_2$ at 50 °C. Mixing time $\tau_m = 0.5$ s. See Fig. 6 for signal labelling.
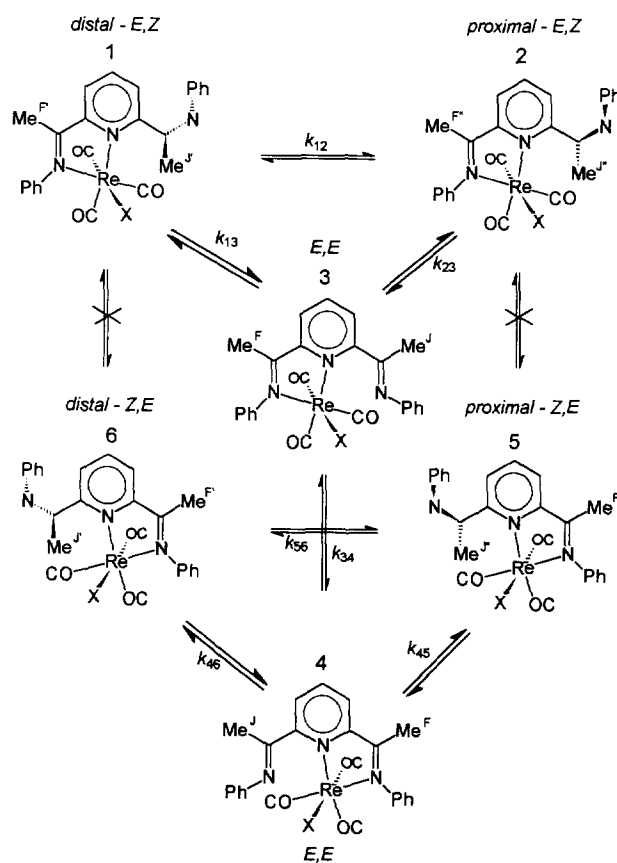

Fig. 6. The exchange pathways between the solution isomers of fac-[ReX(CO)$_3$(BIP)] complexes, defined by the forward first-order rate constants k_{ij}.

Table 7

Rate constants (s⁻¹) derived from 2D-EXSY spectra for fluxional motions on fac-[ReBr(CO)₃(BIP)]

T (°C)	τ_m (s)	$k_{12} = k_{65}$ [a]	$k_{13} = k_{64}$ [b]	$k_{23} = k_{54}$ [c]	k_{34} [d]	$k_{45} = k_{32}$ [e]	$k_{46} = k_{31}$ [f]	$k_{56} = k_{21}$ [g]
30	1.5	0.0147	0.0778	0.0566	0.0821	0.0045	0.0089	0.0210
35	1.5	0.0234	0.1365	0.0715	0.1361	0.0057	0.0156	0.0335
40	1.0	0.0377	0.2328	0.1054	0.2211	0.0084	0.0266	0.0541
45	0.5	0.0764	0.3800	0.2265	0.3476	0.0180	0.0434	0.1097
50	**0.5**	**0.1214**	**0.6608**	**0.3621**	**0.5631**	**0.0288**	**0.0756**	**0.1742**
55	0.2	0.1947	1.0366	0.6031	0.8689	0.0482	0.1140	0.2677

Rate constants in bold script are extracted from the L matrix given in the text.
[a] C–C restricted rotation, distal E,Z → proximal E,Z.
[b] Imine E,Z-isomerisation, distal E,Z → E,E.
[c] Imine E,Z-isomerisation, proximal E,Z → E,E.
[d] 1,4-Metallotropic shift, E,E → E,E.
[e] Imine E,Z-isomerisation, E,E → proximal E,Z.
[f] Imine E,Z-isomerisation, E,E → distal E,Z.
[g] C–C restricted rotation, proximal E,Z → distal E,Z.

and their reverse associates $I_{21} = I_{56}$, $I_{31} = I_{46}$, and $I_{32} = I_{45}$, plus the diagonal signals $I_{11} = I_{66}$, $I_{22} = I_{55}$, and $I_{33} = I_{44}$. In this way the intensity matrix I was constructed as below. After normalising this matrix and constructing the matrix P from the relative populations of the isomers, the D2DNMR [10] program generated the kinetic plus relaxation matrix L. As an example, from the 2D-EXSY spectrum of fac-[ReBr(CO)₃(BIP)], measured at 50 °C with mixing time 0.5 s (Fig. 5), the following I, P and L matrices were generated.

$$I = \begin{bmatrix} 100.0 & 6.75 & 37.04 & 5.46 & 0.0 & 0.0 \\ 6.75 & 79.95 & 16.08 & 2.64 & 0.0 & 0.0 \\ 37.04 & 16.08 & 1082.2 & 296.33 & 2.64 & 5.46 \\ 5.46 & 2.64 & 296.33 & 1082.2 & 16.08 & 37.04 \\ 0.0 & 0.0 & 2.64 & 16.08 & 79.95 & 6.75 \\ 0.0 & 0.0 & 5.46 & 37.04 & 6.75 & 100.0 \end{bmatrix}$$

$$P = \begin{bmatrix} 0.0478783 \\ 0.0333613 \\ 0.4187605 \\ 0.4187605 \\ 0.0333613 \\ 0.0478783 \end{bmatrix}$$

$$L = \begin{bmatrix} -0.9871 & 0.1214 & 0.6608 \\ 0.1742 & -0.7010 & 0.3621 \\ 0.0756 & 0.0288 & -0.6347 \\ 0.0003 & 0.0009 & 0.5631 \\ -0.0009 & -0.0004 & 0.0107 \\ -0.0014 & -0.0006 & 0.0029 \end{bmatrix}$$

$$\begin{bmatrix} 0.0029 & -0.0006 & -0.141 \\ 0.0107 & -0.0004 & -0.0009 \\ 0.5631 & 0.0009 & 0.0003 \\ -0.6347 & 0.0288 & 0.0756 \\ 0.3621 & -0.7010 & 0.1742 \\ 0.6608 & 0.1214 & -0.9871 \end{bmatrix}$$

It should be noted that the I and L matrices are represented in the normal mathematical convention with

their diagonals running from top left to bottom right. This representation corresponds to the experimental spectrum being rotated clockwise from its conventional presentation. Rate constants may be read directly from the off-diagonal elements of the matrix. Choice of τ_m values and treatment of errors followed the literature [10]. Rate data for this and other temperatures for this compound are listed in Table 7.

2.3.2. ¹³C DNMR study

The ¹H and ¹³C NMR spectra at 263 K of the three complexes (Tables 4 and 6) revealed different chemical shifts for the pair of ortho environments of the phenyl ring attached to the metal-coordinated N atom. This suggested restricted rotation of this phenyl ring, which was confirmed by a variable temperature ¹³C study of the signals of C_2 and C_6. On warming, both signals broadened and eventually coalesced at 363 K, the maximum temperature reached. Band shapes for these carbons were fitted for five temperatures between 283 and 363 K using the iterative DNMR5 program, and activation parameters were evaluated. These were as follows; $\Delta H^{\neq} = 54.8 \pm 2.6$ kJ mol⁻¹, $\Delta S^{\neq} = -41 \pm 8$ J K⁻¹ mol⁻¹, $\Delta G^{\neq} = 67.3 \pm 0.2$ kJ mol⁻¹.

3. Discussion

Four different fluxional motions were observed for the complexes fac-[ReX(CO)₃(BIP)], namely (i) 1,4-metallotropic shifts, (ii) E,Z-isomerisation of the pendant imine function, (iii) C–C restricted rotation of the pendant part of the BIP ligand, and (iv) restricted rotation of the phenyl ring attached to the metal-bound nitrogen.

The mechanism of the metal commutation in the

E,E-isomer was deduced by observing the effects of the exchange on the carbonyl signals of the ReX(CO)₃ moiety. Thus, ^{13}C NMR spectra of fac-[ReI(CO)₃(BIP)] were recorded in (CDCl₂)₂ in the temperature range 30 to 130 °C (Fig. 7). The spectra show evidence of the exchange of the equatorial pair while the axial carbonyl signal remains sharp in the range of temperatures studied. This implies that the mechanism proceeds via an intermediate in which the BIP ligand is quasi-terdentate. Some recent studies of ours on metal complexes of a 2,2':6',2"-terpyridine have shown that this so-called 'tick–tock' twist mechanism is truly associative, involving coordination of all three N donors in the transition state [11]. We postulate an analogous mechanism in the present complexes.

E,Z-isomerisation in the pendant imine bond can proceed through a 180° rotation about the C=N double bond, or through an inversion of the nitrogen [4]. On the basis of previous studies [4,12] the favoured mechanism is an inversion process.

The rate data acquired in the 2D-EXSY studies were obtained over a rather limited temperature range (typically 303–328 K). In order to check on the reliability of the rate constants, extrapolations were made into the higher temperature range where dynamic broadening of the 1D spectra was observed (e.g. 325–415 K, Fig. 4).

The extrapolated rate constants were then used to simulate the dynamically broadened methyl signals and the simulated spectra compared digitally using the DNMR5 program with the experimental spectra and iterated until the best fits were obtained. In all cases the iterated rate constants were very close in magnitude to those predicted from the 2D-EXSY experiments. Activation energy data (Table 8) were calculated from the combined 2D-EXSY and DNMR5 derived rate constants and are based on least-squares fittings of Eyring plots.

By inspection of the $\Delta G^{\neq}$ values for the metallotropic shift (Table 8) it can be concluded that there is no apparent halogen dependency in this fluxional motion. However, the isomerisation distal $E,Z \rightleftharpoons E,E$ does seem to be slightly halide dependent. The magnitudes of $\Delta G^{\neq}$ are generally lower for the metallotropic shift than for the other processes, but the differences are small and all $\Delta G^{\neq}$ values fall in the range 79–88 kJ mol^{-1}. $\Delta G^{\neq}$ values for the forward and reverse directions of a given process reflect the relative ground state populations of the interconverting species.

The main conclusions of this work on [ReX(CO)₃(BIP)] complexes are:

(i) these complexes are highly stereochemically nonrigid in solution, undergoing intramolecular 1,4-metallotropic shifts, E,Z-isomerisation of the pendant imine
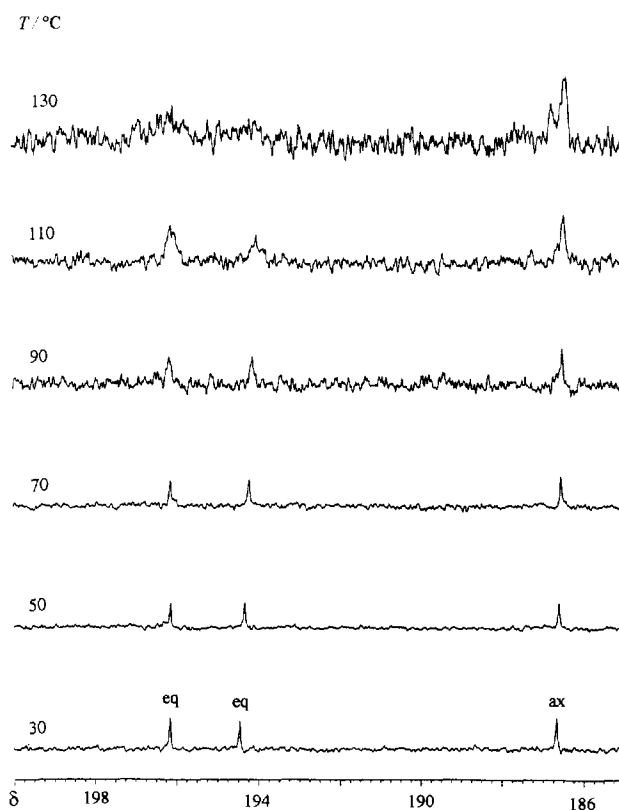

Fig. 7. 100 MHz ^{13}C NMR spectra (carbonyl region) of fac-[ReI(CO)₃(BIP)] in (CDCl₂)₂ in the temperature range 30–130 °C, showing the effect of the 1,4-metallotropic shift.

Table 8
Activation parameters for fluxional processes in fac-[ReX(CO)$_3$(BIP)] (X = Cl, Br, I) complexes derived from combined data obtained from 2D-EXSY spectra and 1D band shape analysis

Compound	Process	k_{ij} [e]	$\Delta H^{\ddagger}$ (kJ mol⁻¹)	$\Delta S^{\ddagger}$ (J mol⁻¹ K⁻¹)	$\Delta G^{\ddagger}$ [f] (kJ mol⁻¹)
[ReCl(CO)₃(BIP)]	a		75.14 ± 1.84	−14.8 ± 5.2	79.55 ± 0.28
	b	f	80.41 ± 0.97	−13.9 ± 2.8	84.54 ± 0.14
		r	81.39 ± 2.63	−8.8 ± 7.6	84.02 ± 0.37
	c	f	84.43 ± 1.46	9.0 ± 4.2	80.74 ± 0.21
		r	86.70 ± 0.87	0.2 ± 2.5	86.64 ± 0.12
	d	f	87.95 ± 1.57	16.4 ± 4.5	83.08 ± 0.22
		r	83.46 ± 1.96	−14.6 ± 5.6	87.81 ± 0.28
[ReBr(CO)₃(BIP)]	a		75.55 ± 0.53	−16.3 ± 1.5	80.42 ± 0.07
	b	f	88.69 ± 1.21	11.4 ± 3.5	85.30 ± 0.17
		r	81.06 ± 2.56	−9.3 ± 7.4	83.84 ± 0.35
	c	f	86.11 ± 1.08	17.7 ± 3.1	80.85 ± 0.15
		r	84.96 ± 1.13	−4.0 ± 3.3	86.17 ± 0.16
	d	f	84.21 ± 0.99	7.0 ± 2.9	82.11 ± 0.14
		r	84.26 ± 1.58	−13.7 ± 4.6	88.36 ± 0.22
[ReI(CO)₃(BIP)]	a		77.02 ± 0.39	−12.2 ± 1.1	80.67 ± 0.06
	b	f	83.36 ± 3.06	−8.1 ± 8.8	85.78 ± 0.44
		r	85.16 ± 3.24	2.8 ± 9.3	84.32 ± 0.46
	c	f	82.98 ± 0.17	11.0 ± 2.0	79.70 ± 0.10
		r	88.47 ± 0.87	6.1 ± 2.5	86.65 ± 0.12
	d	f	85.00 ± 0.49	16.6 ± 1.5	80.04 ± 0.06
		r	81.59 ± 1.26	−21.3 ± 3.6	87.94 ± 0.18

[a] 1,4-Metallotropic shift in E,E complex.
[b] Restricted C–C rotation of the pendant part of the BIP ligand for the minor species, distal $E,Z \rightleftharpoons$ proximal E,Z.
[c] E,Z-isomerisation, proximal $E,Z \rightleftharpoons E,E$.
[d] E,Z-isomerisation, distal $E,Z \rightleftharpoons E,E$.
[e] f = forward, r = reverse process.
[f] Measured at 298.15 K.

function of the ligand, and restricted C–C rotation of the pendant arm of the BIP ligand;

(ii) these three processes constitute a six-site exchange problem which has been treated quantitatively by NMR 2D-EXSY experiments;

(iii) rates and activation energies of these three types of processes are of comparable magnitude;

(iv) rotation of the phenyl ring attached to the metal-coordinated nitrogen is restricted, but its activation energy is considerably lower than the energies for the other three dynamic processes.

4. Experimental

4.1. Physical measurements

Elemental analyses were carried out by Butterworth Laboratories (Teddington, Middlesex, London). Melting points were recorded in air on a Gallenkamp melting point apparatus and are uncorrected. Mass spectra were recorded on a Kratos Profile HV-3 spectrometer operating in liquid secondary ion mass spectrometry (LSIMS) mode using a 3-nitro-benzyl alcohol matrix. Infrared spectra were recorded as CHCl$_3$ solutions using CaF$_2$

solution cells on a Perkin–Elmer 881 spectrometer. NMR spectra were recorded on a Bruker DRX400 instrument operating at 400.13 MHz for ^{1}H and at 100.61 MHz for ^{13}C. ^{1}H and ^{13}C{^{1}H} chemical shifts are quoted relative to Me$_4$Si (TMS). A standard B-VT 2000 variable temperature unit was used to control the probe temperature, the calibration of this unit being checked periodically against a Comark digital thermometer. The temperatures are considered to be accurate to ± 1 °C. ^{1}H–^{13}C correlation spectra and COSY spectra were obtained with the Bruker automation programs INVBTP and COSY45. 2D-EXSY spectra were obtained with the Bruker automation program NOESYTP. The initial delay time was typically 2.00 s, the evolution time was initially 3 × 10⁻⁶ s, and the mixing time was varied according to the experimental temperature.

Kinetic data were derived from band shape analysis of ^{1}H NMR spectra using the iterative DNMR5 program [13] for the simulation of band shapes, and from 2D-EXSY spectra using the D2DNMR [10] program. Appropriately averaged intensity values using row integration of the 2D-EXSY spectra were used to calculate the rate constants. Activation parameters were calculated from a least-squares fit of the Arrhenius and Eyring plots. Quoted errors are statistical errors based on scattering of the rate constants around the straight line only.

4.2. Materials

Previously described methods were used to prepare the complexes [ReX(CO)$_5$] (X = Cl, Br, and I) [14,15]. The ligand 2,6-bis[1-(phenylimino)ethyl]pyridine (BIP) was prepared by condensation of 2,6-diacetylpyridine with aniline in benzene [16].

4.2.1. fac-[ReX(CO)$_3$(BIP)] (X = Cl and Br)

Rheniumpentacarbonylchloride (0.10 g, 0.28 mmol) and BIP (0.09 g, 0.30 mmol) were heated under reflux in benzene (10 cm^3) for 2.5 h. Petroleum (b.p. 40–60 °C, 10 cm^3) was added to the hot solution. After allowing the solution to stand at ambient temperature for 9 h, red–orange crystals were separated and washed with portions of petroleum (2 × 30 cm^3). The sample was then dried in vacuum for 7 h. Yield 0.15 g, 86.7%. The same procedure was followed for fac-[ReBr(CO)$_3$(BIP)], affording red–orange crystals. Yield 0.145 g, 91.5%.

4.2.2. fac-[ReI(CO)$_3$(BIP)]

Rheniumpentacarbonyliodide (0.35 g, 0.77 mmol) and BIP (0.25 g, 0.80 mmol) were heated under reflux in benzene (30 cm^3) for 16 h. The solvent was evaporated under reduced pressure to 5 cm^3. A precipitate was obtained by adding hexane (20 cm^3). After filtration the orange–red powder was washed with a further portion of hexane (20 cm^3) and dried under vacuum for 7 h. Yield 0.15 g, 95.7%.

4.3. Crystal structure determination of [ReBr(CO)$_3$(BIP)]

Crystal data. C$_{24}$H$_{19}$BrN$_3$O$_3$Re, M = 663.53, triclinic, a = 8.240(2), b = 12.294(8), c = 12.666(8) Å, α = 67.211(8), β = 86.048(10), γ = 79.37(2)°, U = 1162.8(9) Å^3, λ = 0.71069 Å, space group P$\bar{1}$, Z = 2, D$_c$ = 1.895 g cm^{-3}, F(000) = 636, μ = 69.74 cm^{-1}, T = 120 K.

The X-ray measurements were made on a crystal of approximate dimensions 0.20 × 0.14 × 0.08 mm^3 which was mounted using silicone oil and then transferred to the goniostat. The data were collected at 120 K using Mo Kα radiation (λ = 0.71069 Å, graphite monochromator) on a Delft Instruments FAST TV area detector diffractometer equipped with a rotating anode generator (50 kV, 50 mA), a buffer-board, a DEP image intensifier, and an Oxford Cryostream low-temperature cooling system by following previously described procedures [17]. The cell parameters were obtained by least-squares refinement of the diffractometer angles for 250 reflections within θ ranges 1.74–24.77°. A total 4729 intensities were collected within the same θ range from an area corresponding to slightly more than a hemisphere of reciprocal space [index range −9 ≤ h ≤ 8,

−14 ≤ k ≤ 14, −14 ≤ l ≤ 14] which gave 3147 (R$_{int}$ = 0.0472) unique data with intensities greater than zero. The data were corrected for Lorentz and polarisation factors, and also for absorption effects using the program DIFABS [18]. The absorption correction factors ranged from 0.884–1.019.

The structure was solved by Patterson methods (SHELXS86) [19] and difference electron density syntheses, and refined on F^2 by full-matrix least-squares (SHELXL93) [20] using all unique data. The non-hydrogen atoms were anisotropic. The hydrogen atoms were included in calculated positions (riding model) with U$_{iso}$ = nU$_{eq}$ of the parent carbon (n = 1.2 for CH and 1.5 for CH$_3$ groups). The maximum residual electron densities in the final difference maps were close to the Re atom [1.86 e Å^{-3}] and indicated no features of stereochemical significance. The final R [= Σ(ΔF)/Σ(F$_o$)] and R$_w$ (= [Σ{w(Δ(F^2)^2)}/Σ{w(F$_o^2$)^2}]$^{1/2}$) values were 0.0423 and 0.1046 respectively, for all unique data and 291 parameters. The corresponding R values for 2967 data with I > 2σ(I) were 0.0406 and 0.1041 respectively. The goodness-of-fit on F^2 was 1.116. The weighting scheme w = 1/[σ^2(F$_o$)^2 + (0.0716*P)^2], with P = [Max(F$_o^2$) + 2*F$_c^2$]/3, was used which gave satisfactory agreement analyses. Sources of scattering factors as in Ref. [20]. The calculations were done on a Pentium P5-90 personal computer. Fractional atom coordinates, interatomic distances and angles are presented in Tables 2 and 3.

References

[1] E.W. Abel, V.S. Dimitrov, N.J. Long, K.G. Orrell, A.G. Osborne, H.M. Pain, V. Šik, M.B. Hursthouse and M.A. Mazid, J. Chem. Soc., Dalton Trans., (1993) 597.

[2] E.R. Civitello, P.S. Dragovitch, T.B. Karpishin, S.G. Novick, G. Bierach, J.F. O'Connell and T.D. Westmoreland, Inorg. Chem., 32 (1993) 237.

[3] E.W. Abel, K.A. Hylands, M.D. Olsen, K.G. Orrell, A.G. Osborne, V. Šik and G.N. Ward, J. Chem. Soc., Dalton Trans., (1994) 1079.

[4] K.G. Orrell, A.G. Osborne, V. Šik and M. Webba da Silva, J. Organomet. Chem., 530 (1997) 237.

[5] J.M. Albon, D.A. Edwards and P.J. Moore, Inorg. Chim. Acta, 159 (1989) 19.

[6] G.J. Stor, M. van der Vis, D.J. Stufkins, A. Oskam, J. Fraanje and K. Goubitz, J. Organomet. Chem., 482 (1994) 15.

[7] E.C. Alyea, G. Ferguson and R.J. Restivo, Inorg. Chem., 14 (1975) 2491.

[8] D.A. Edwards, M.F. Mahon, W.R. Martin, K.C. Molloy, P.E. Fanwick and R.A. Walton, J. Chem. Soc., Dalton Trans., (1990) 3161.

[9] E.W. Abel, K.G. Orrell, A.G. Osborne, H.M. Pain, V. Šik, M.B. Hursthouse and K.M.A. Malik, *J. Chem. Soc., Dalton Trans.,* (1994) 3441.

[10] E.W. Abel, T.P.J. Coston, K.G. Orrell, V. Šik and D. Stephenson, *J. Magn. Res., 70* (1986) 34.

[11] E.W. Abel, A. Gelling, K.G. Orrell, A.G. Osborne and V. Šik, *J. Chem. Soc., Chem. Commun.,* (1996) 2329.

[12] R. Knorr, J. Ruhdorfer, J. Mehlstäubl, P. Böhrer and D.S. Stephenson, *Chem. Ber., 126* (1993) 747.

[13] D.S. Stephenson and G. Binsch, *J. Magn. Res., 32* (1978) 145.

[14] H.D. Kaesz, R. Bau, D. Hendrickson and J.M. Smith, *J. Am. Chem. Soc., 89* (1967) 2844.

[15] M.M. Bhatti, *Ph.D. Thesis,* University of Exeter, 1980.

[16] A.J. Blake, A.J. Lavery, T.J. Hyde and M. Schroder, *J. Chem. Soc., Dalton Trans.,* (1989) 965.

[17] J.A. Darr, S.R. Drake, M.B. Hursthouse and K.M.A. Malik, *Inorg. Chem., 32* (1993) 5704.

[18] N.P.C. Walker and D. Stuart, *Acta Crystallogr., A39* (1983) 158; adapted for FAST geometry by A.K. Karaulov, University of Wales, 1991.

[19] G.M. Sheldrick, *Acta Crystallogr., A46* (1990) 467.

[20] G.M. Sheldrick, SHELXL93, *Program for Crystal Structure Refinement,* University of Gottingen, Germany, 1993.